

Detector for imaging of explosions: present status and future prospects with higher energy X-rays.

Aulchenko V.M.^a, Evdokov O.V.^b, Shekhtman L.I.^{a*}, Ten K.A.^c, Tolochko B.P.^b, Zhogin I.L.^b, Zhulanov V.V.^a

^a*Budker Institute of Nuclear Physics*

11 Lavrentiev Avenue, Novosibirsk 630090

Russia. Fax: 7(383)3307163,

e-mail: L.I.Shekhtman@inp.nsk.su

^b*Institute of Solid-State Chemistry and Mechano-Chemistry*

630090 Novosibirsk, Russian Federation

^c*Lavrentiev Institute of Hydrodynamics*

630090 Novosibirsk, Russian Federation

ABSTRACT: The detector for imaging of explosions (DIMEX) is in operation at the synchrotron radiation (SR) beam-line at VEPP-3 electron ring at Budker INP since 2002. DIMEX is based on one-coordinate gas ionization chamber filled with Xe-CO₂(3:1) mixture at 7atm, and active Frisch-grid made of Gas Electron Multiplier (GEM). The detector has spatial resolution of ~ 0.2 mm and dynamic range of ~ 100 that allows to realize the precision of signal measurement at a percent level. The frame rate can be tuned up to 8 MHz (125 ns per image) and up to 32 images can be stored in one shot. At present DIMEX is used with the X-ray beam from 2T wiggler that has ~ 20 keV average energy. Future possibility to install similar detector at the SR beam-line at VEPP-4 electron ring is discussed.

KEYWORDS: GEM, X-ray detector, detector modelling and simulations.

*Corresponding author

Contents

1. Introduction.	1
2. Present status of DIMEX at VEPP-3.	1
3. Prospects of DIMEX with higher energy SR at VEPP-4M.	5
4. Conclusions.	11

1. Introduction.

The detector for imaging of explosions (DIMEX) is in operation at the synchrotron radiation (SR) beam-line at VEPP-3 electron ring at Budker INP since 2002 ([1], [2], [3]). DIMEX is used for the studies of material properties in the conditions with very high temperatures and pressures (i.e. during detonation) as well as of the processes of formation of new materials (including nano-structures) during an explosion ([4], [5]). The studies are performed either by the measurements of absorption of the SR beam by an exploding sample (direct absorption experiments), or by the measurements of photon flux scattered at small angles from an exploding sample (SAXS experiments). In both types of experiments DIMEX allows the measurement of one-coordinate distribution of the X-ray flux emitted by a single electron bunch and then either partially absorbed or scattered by a sample. The detector measures a sequence of up to 32 of such images corresponding to subsequent bunches. Thus the effective time resolution of the method is determined by the length of an electron bunch in the accelerator and is below 1ns.

At present DIMEX is operating at the beam-line with white SR beam from 2T wiggler with average energy of photons around 20keV (after passing through Be windows (5mm) and the sample (1cm of explosive)) [1]. This low energy imposes limit on the sample thickness of ~ 1 cm because otherwise the absorption in the sample becomes too strong and limited statistics of transmitted photons does not allow to get necessary precision of the measurement. Higher energy of SR beam can be obtained at VEPP-4M with 5-pole 1.3T wiggler that is now under development. The dedicated simulation study has been performed to get estimates of the main parameters of DIMEX for the X-ray spectrum at VEPP-4M. The present paper describes current status of DIMEX performance at VEPP-3 and summarizes the results of simulation studies of possible operation at VEPP-4M.

2. Present status of DIMEX at VEPP-3.

DIMEX is based on the high pressure gas ionization chamber with active Frisch-grid made of gas electron multiplier (GEM). Design of the detector is shown schematically in Fig. 1. X-ray beam enters the detector box through carbon fiber window and is absorbed in the gap between the drift

electrode and top GEM side. Electrons of primary ionization drift towards GEM, partially penetrate through it and then drift through the gap between bottom GEM side and strip board (induction gap). During the last phase the electrons induce charge at the strips (strip pitch is 0.1mm). Detector is filled with Xe-CO₂ (3:1) mixture at 7 atm (absolute).

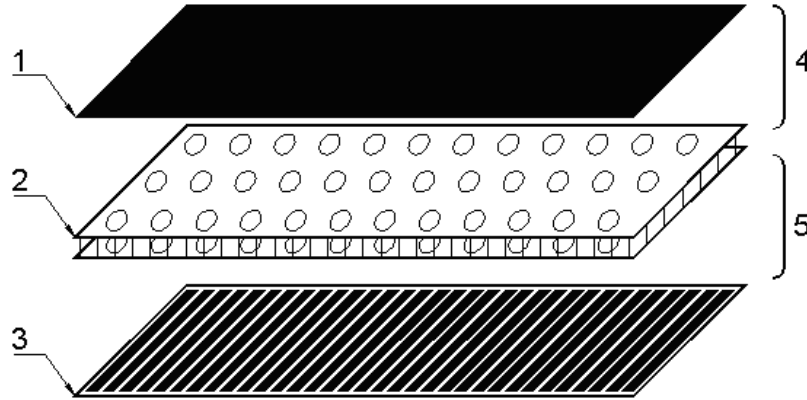


Figure 1. Schematic view of DIMEX design . 1 - drift electrode, 2 - GEM, 3 - strip board, 4 - drift gap, 5 - induction gap.

Each strip of the anode board is connected to the input of the integrator chip APC128 [6]. This chip contains 128 channels with integrator and 32-cell analogue pipeline in each channel. The charge from the integrator can be stored in any of the pipeline cells. The pipeline can be read out through the analogue multiplexer. The pipeline switching and readout frequency can be up to 10MHz.

GEM shields the strip board from the charge induction from positive ions and absorbs part of the electrons passing through thus reducing the signal from each photon. As the dynamic range of the APC128 integrator is limited, the reduction of charge induced per single photon increases effectively the dynamic range in terms of photons. At present the GEM transparency is about 0.5 with the drift field of 16kV/cm, induction field of 8kV/cm and GEM voltage of 800V (for example, see data from [7] and [8]). The transparency can be changed within a certain limits and thus the dynamic range can be tuned. However we have not yet tried this option.

Detailed description of the operation algorithm of DIMEX can be found in [3]. The detector is opened to the beam for $\sim 60\mu\text{s}$ by a special rotation shutter and explosion is triggered during this time gap. The exact synchronization between the detonation and the detector timing sequence is achieved with the help of two wires embedded into the explosive. The wires are shorted when the detonation wave is passing through them.

Bunch crossing time of VEPP-3 synchrotron is 250ns in 1-bunch regime. The accelerator can also operate in 2-bunch mode. The timing sequence of DIMEX is synchronized with the bunch crossing. Data from up to 32 bunches can be stored separately in the pipeline cells. After recording the data from 32 bunches the detector sequence is stopped and data from the pipeline is transferred to the computer through 100Mb/s ethernet line.

Spatial resolution of DIMEX is determined mostly by pressure of the operating gas mixture. The line spread function measured by the edge method is shown in Fig. 2. The resolution (FWHM) is close to 0.2mm.

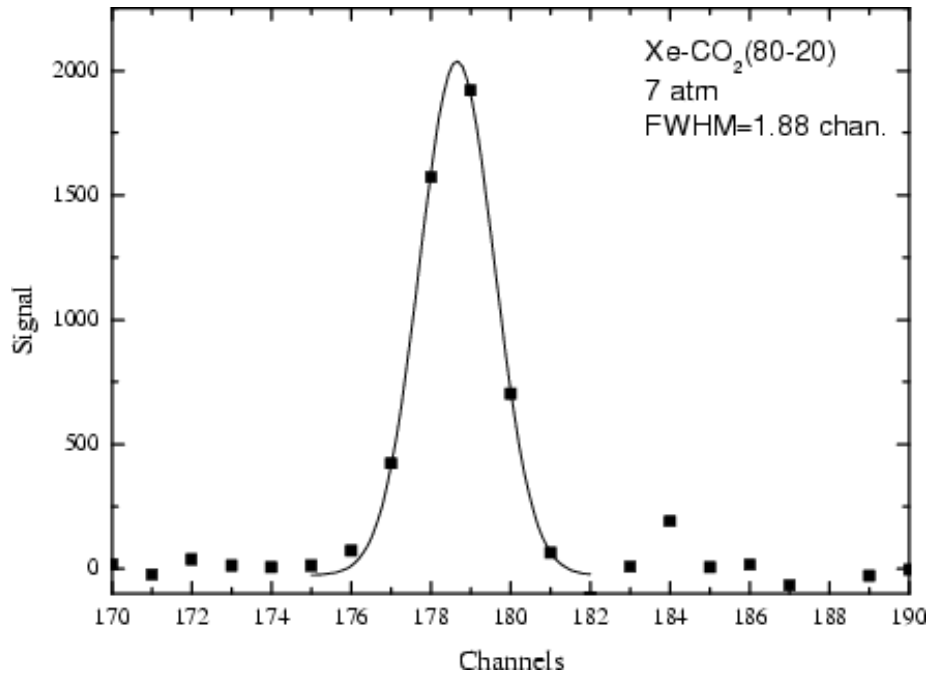


Figure 2. The image of thin beam (line spread function) measured with the edge method.

Signal and signal to noise ratio as a function of incident flux, calculated from the known electron beam energy, current and B-field of the wiggler¹ are shown in Fig. 3. Signal to noise ratio reaches ~ 100 demonstrating the possibility of signal measurement at a percent level of precision. The maximal signal is limited by the space charge accumulation due to slow positive ions in the drift gap.

The result of one of the direct absorption experiments is shown in Fig. 4, where the density map of the exploding sample is reconstructed [4]. The data are reconstructed from the time evolution of the transmitted signal in one slice, assuming constant speed of the detonation wave. In the figure we can see the undistorted sample at $Z < -5\text{mm}$ with the density of $\sim 1.5\text{g/cm}^3$. At $Z = -5\text{mm}$ the density jumps above $\sim 2.0\text{g/cm}^3$ due to the detonation and then the sample is decaying with the density steadily decreasing. The most important observation in this kind of experiments is the value of density increase behind the detonation wave, and the exact density profile at the moment of detonation.

SAXS experiments can give information about the amount and size of particles that are produced in an explosion. The example of SAXS experiment is shown in Fig. 5 and Fig. 6 [5]. In Fig. 5 the angular distribution of scattered X-rays is shown $3\mu\text{s}$ after the detonation wave passed through the slice of the sample exposed to the beam. In Fig. 6 the whole evolution of SAXS angular distribution in time is shown. We can see that SAXS intensity is growing with time for quite a long period after the detonation.

After the first years of DIMEX operation the power of the method of imaging of the radiation from single electron bunch has become obvious. However further improvement of the detector is

¹Calculated with XOP2.0

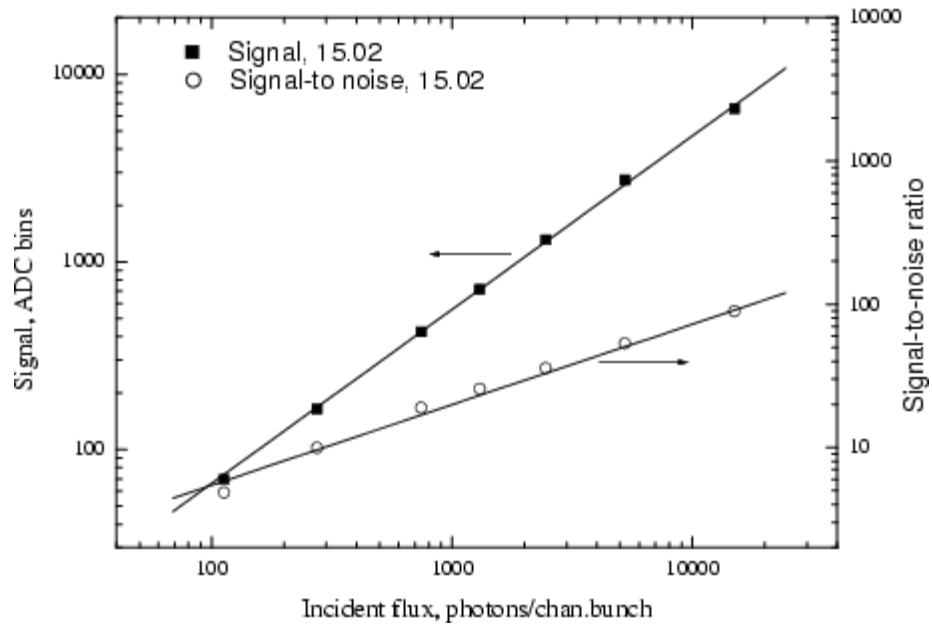


Figure 3. Signal (left scale) and signal to noise ratio (right scale) as a function of the X-ray flux at the entrance window of the detector.

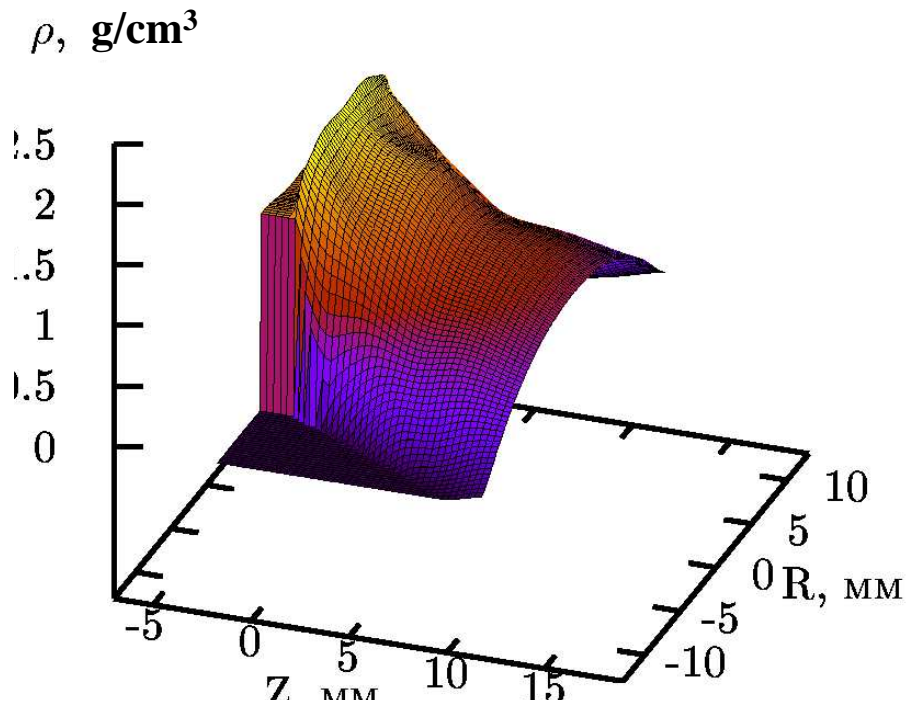


Figure 4. Reconstructed density map of the exploding sample.

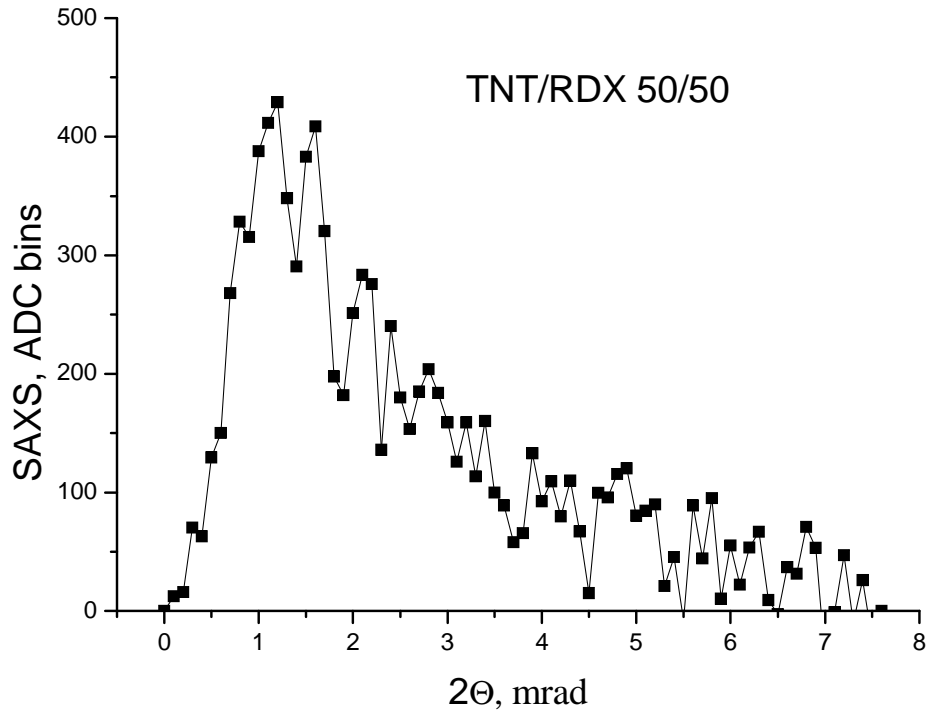


Figure 5. SAXS experiment with the explosion of composite sample. Angular distribution of SAXS radiation $3\mu\text{s}$ after the passage of detonation wave.

necessary. For the direct absorption experiments the improvement of spatial resolution is needed down to $50\mu\text{m}$ and below as well as the increase of dynamic range and the precision of signal measurement. For both SAXS and direct absorption experiments the higher frame rate would be useful that is however limited by the bunch timing of the accelerator. Also for both SAXS and direct absorption experiments the transition to higher X-ray energies would be useful. Higher X-ray energies will allow to study thicker samples with higher densities.

3. Prospects of DIMEX with higher energy SR at VEPP-4M.

The energy spectrum of radiation from the 5-pole 1.3T wiggler that is now under development for VEPP-4M ring, is shown in Fig. 7². The figure presents the primary spectrum, the spectrum after absorption in Be windows with total thickness of 5mm and the spectrum after absorption in 20mm of explosive (dashed line, below will be referred as spectrum 3, pure carbon at a density of $1.6\text{g}/\text{cm}^3$ has been taken as an explosive). We can see that spectrum 3 has maximum at $\sim 30\text{keV}$. At around 50 keV its spectral density is about half of the maximum and the tail spreads up to 100 keV.

The efficiency of detector with 1mm carbon fiber window of $1.2\text{g}/\text{cm}^3$ density, dead zone of gas 3mm in depth and 30mm deep sensitive zone, is shown in Fig. 8 as a function of X-ray energy. The efficiency has been calculated for the gas mixture of Xe-CO₂(3:1) at 7atm absolute pressure

²Spectrum is calculated with XOP2.0

TNT/RDX 50/50 I=62 mA

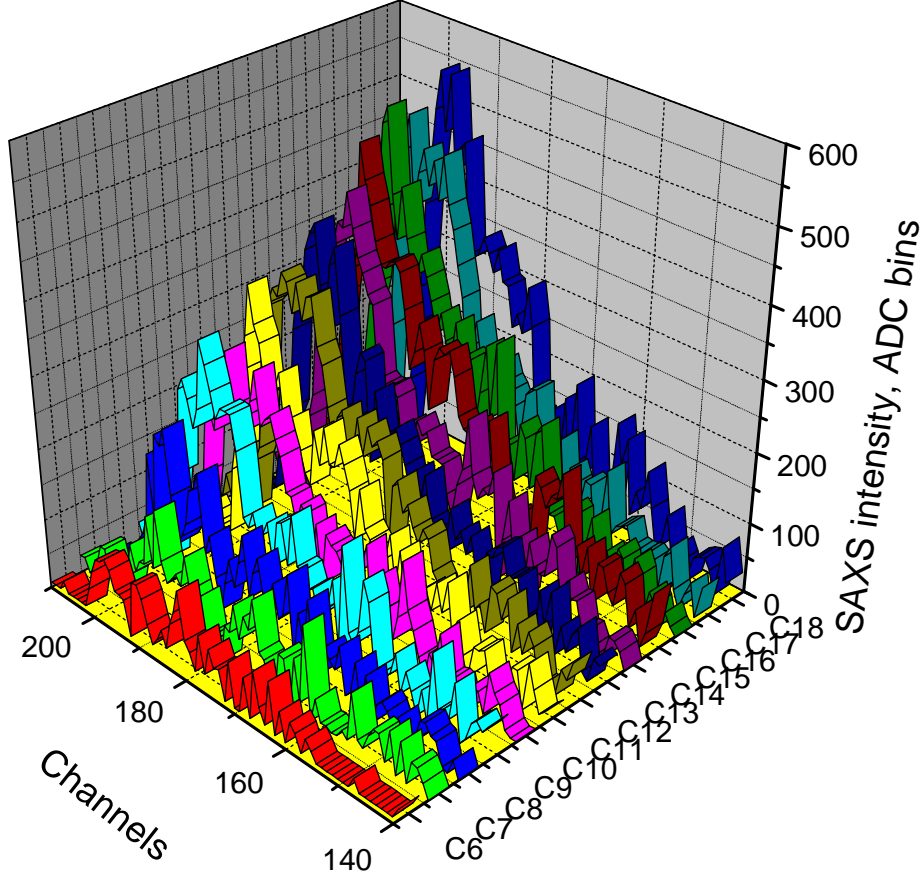


Figure 6. Time evolution of the angular distribution of SAXS. Images from different frames have different colors. Frame rate is 2MHz.

(calculation has been performed with XOP2.0). By efficiency we mean here the probability of absorption of X-ray photon in the sensitive region of the detector.

The efficiency of DIMEX to photons with spectrum 3 has been calculated by Monte-Carlo simulation. Photon flux distributed uniformly along the direction of entrance window was directed perpendicular to the window plane. The photons energy was distributed according to spectrum 3. Photons that entered the detector volume have released their energy partly or totally in the dead zone or in the sensitive region. Part of the photon flux transferred through the detector volume without interaction. The simulation has been performed with FLUKA2006.3 package [9], [10]. In order to determine the probability of interaction in the sensitive region the number of photons entering this region have been detected as well as the number of primary photons leaving the sensitive region without interaction. The difference between the former and the latter normalized by the number of primary photons has given the efficiency.

Apart from the probability of interaction of photons distributed following spectrum 3, the simulation has given the value of detective quantum efficiency(DQE) that characterizes the possibility to detect small deviations of signal at noisy background and with limited photons statistics [11], [12]. DQE can be determined as a square of signal to noise ratio normalized to the input flux

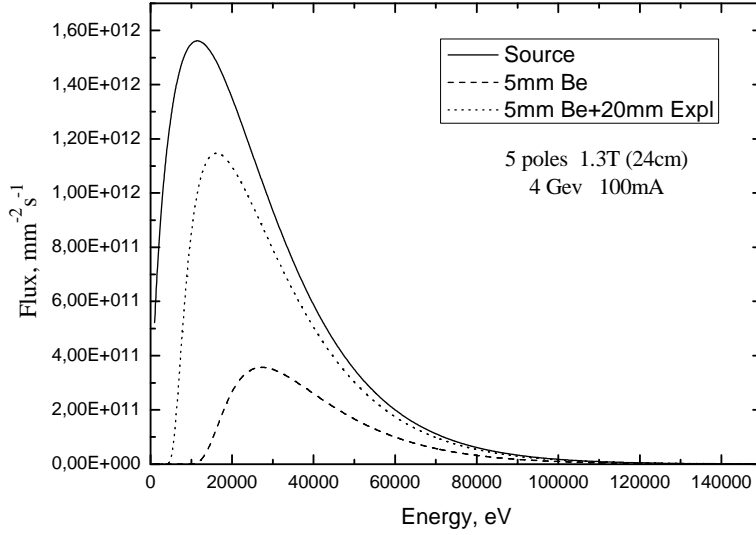


Figure 7. Spectrum of radiation from 5-pole 1.3T wiggler at VEPP-4M.

(in photons per channel) and to the correlation interval X_{corr} (in channels), where X_{corr} is FWHM of the autocorrelation function.

$$DQE = (s/n)^2 / (N \cdot X_{corr}) \quad (3.1)$$

For the calculation of DQE the distribution of energy deposited in the sensitive region along the direction of the input window has been simulated. Uniform X-ray flux has been falling onto the detector within 1cm region along the input window. The whole region has been divided into 200 $50\mu\text{m}$ intervals. The rms and mean values of energy deposited in these intervals have been calculated. The former has been taken as noise and the latter as signal value. The input flux has been known from simulation conditions. For the simulation of the autocorrelation function the pencil-like beam has been used with all the photons entering detector at a constant coordinate. As a result the line-spread function (LSF) of the detector has been obtained (see Fig. 13). The autocorrelation function is a square of LSF. As a result of simulation the efficiency obtained is equal to 59% and DQE is equal to 48%. DQE is less than the probability of absorption in the sensitive region because of fluctuations of energy deposited after the photons absorption.

Spatial resolution of DIMEX has been characterized by LSF that was obtained by the simulation. Different processes affecting the resolution could be included. In Fig. 9 the comparison between LSF with and without electrons diffusion is shown for the beam of 50keV photons. The drift length in the detector is 2.5mm and the variance of electron position due to diffusion is $33\mu\text{m}$. Fig. 9 demonstrates that spatial resolution of DIMEX is mostly determined by diffusion.

The influence of pressure on the spatial resolution of DIMEX is shown in Fig. 10. The improvement of spatial resolution with pressure is determined by the diffusion that is reversed proportional to square root of pressure. Thus the change of resolution is negligible when pressure is increased from 7atm to 10atm. Further increase of pressure is problematic because of too high voltages that has to be kept on the detector elements (in order to keep constant E/p).

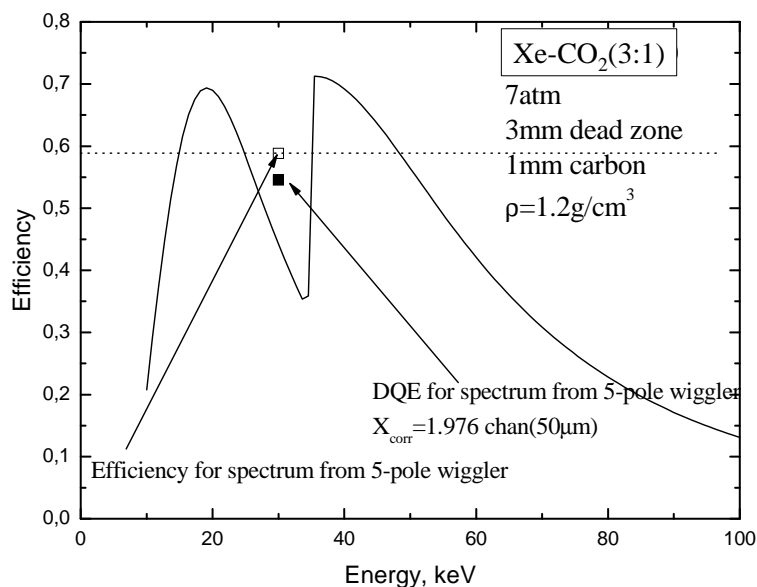


Figure 8. Efficiency as a function of energy. Efficiency and DQE for the radiation with spectrum 3 shown at $E=30\text{keV}$.

Comparison of the spatial resolution at two different energies 20keV and 50keV (Fig. 11) demonstrates that the dependence of LSF on energy is negligible in this energy range. Spatial resolution for X-rays with energy distribution as in spectrum 3 is shown in Fig. 12 in comparison with the spatial resolution for 20 keV photons. The line spread functions in Fig. 11 and 12 are taken without diffusion to observe better the effect of different photon energies. From Fig. 12 we can see that the LSF for 20 keV photons is wider in the central part than the LSF for spectrum 3. It happens due to low energy photoelectrons that are emitted after photo-effect on K-edge of Xe ($\sim 35\text{keV}$). The LSF for spectrum 3 has much wider halo around the central part with long tails as compared to the LSF for 20 keV photons that is formed by long high energy tail of the energy spectrum and by the fluorescent photons that are emitted after the absorption on Xe K-edge.

Complete line spread functions with the diffusion taken into account are compared in Fig. 13 for 20keV photons beam and for X-rays with energy spectrum 3. The difference between these two LSF is only in wider halo for the case of spectrum 3. FWHM in both cases is about $170\mu\text{m}$ that fits very well with the experimental result (see Fig. 2).

An alternative to the gaseous detector can be a solid-state device. Fig. 14 shows the probability of interaction through Compton scattering (at least one time), photo-absorption and total probability of interaction in 1cm of silicon as a function of X-ray energy. Below 30keV the probability of photon absorption is close to 1. Compton scattering occurs with probability of $\sim 30\%$ in the energy range from 20keV to 100keV. The efficiency (probability of absorption or at least one scattering) for radiation with spectrum 3 is also shown in the figure as well as DQE for the same kind of X-rays.

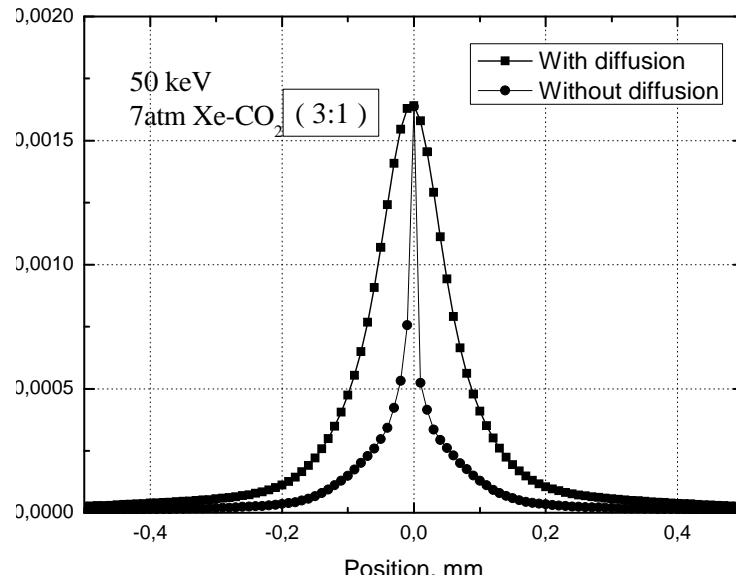


Figure 9. Line spread function for 50keV X-rays. Comparison of the cases with diffusion and without diffusion.

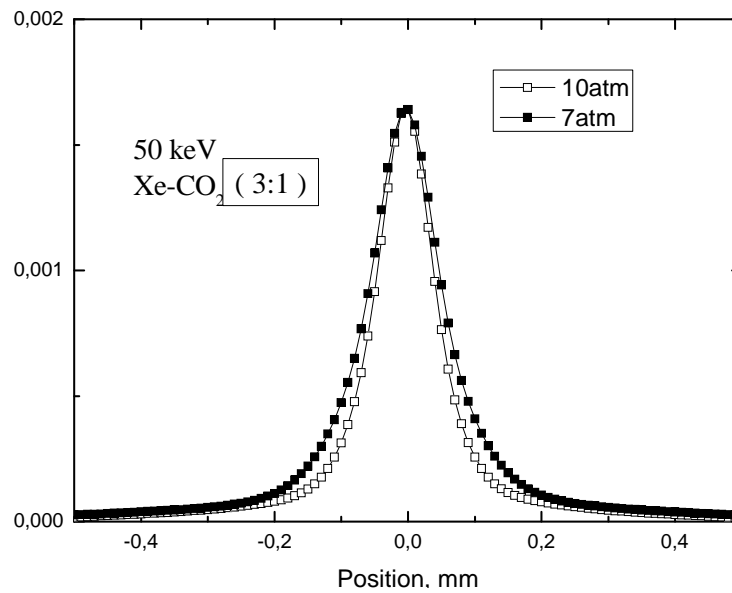


Figure 10. Modification of LSF with pressure.

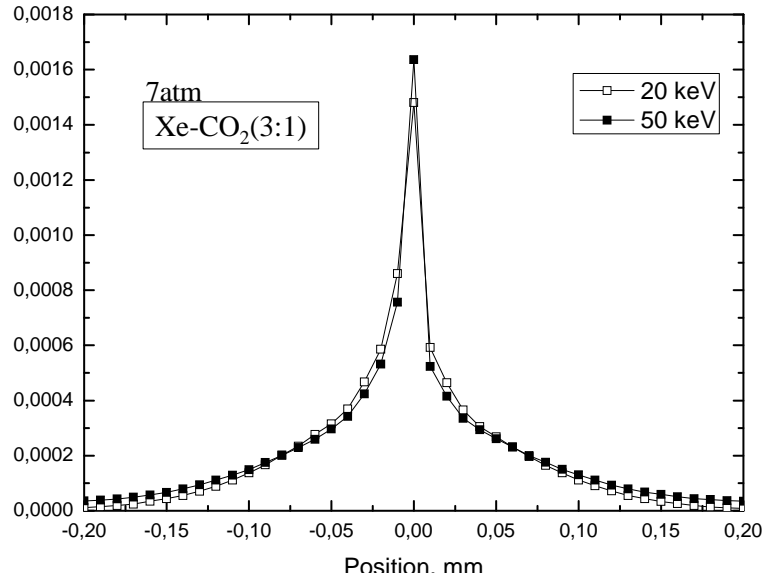


Figure 11. Comparison of LSF for 20keV and 50keV photons. LSF is simulated without diffusion.

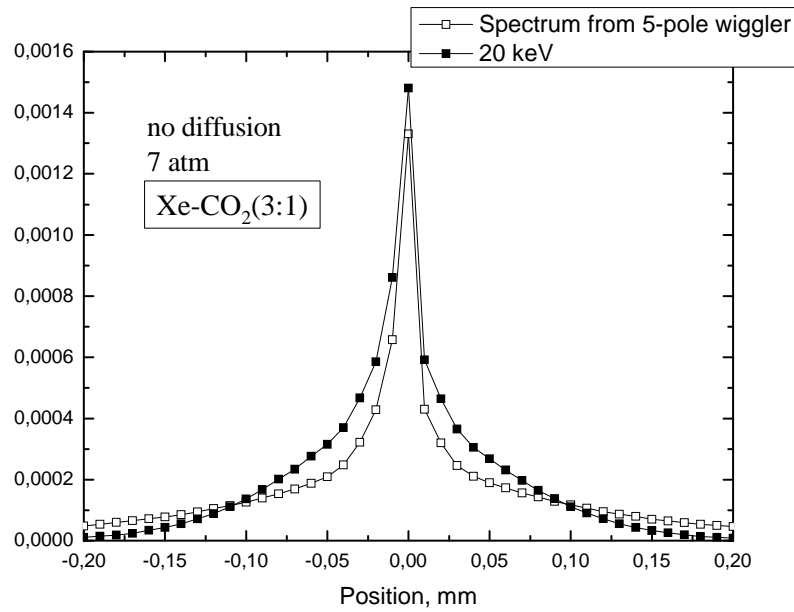


Figure 12. Comparison of LSF for 20keV photons and photons with energy spectrum 3 without diffusion.

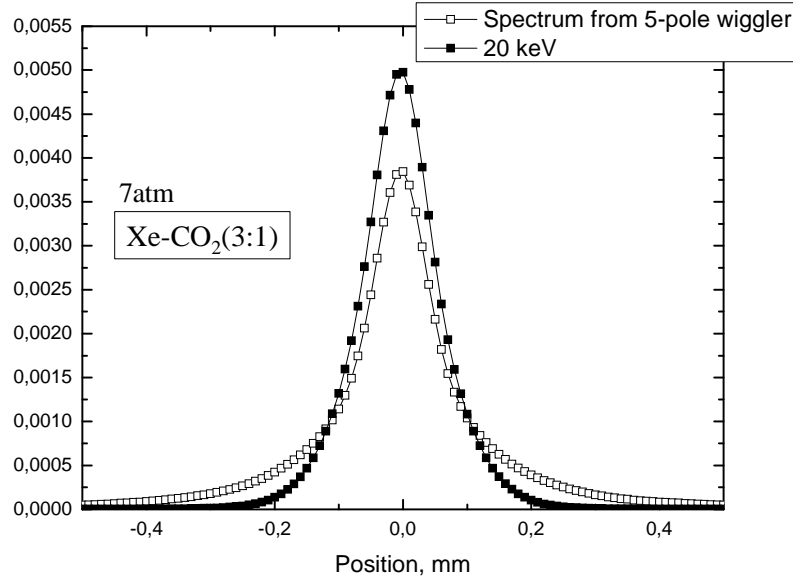


Figure 13. Comparison of LSF for 20keV photons and photons with energy spectrum 3 with diffusion.

As Compton scattering causes energy deposition through a recoil electron, this process has been accounted for in the efficiency calculation. The energy deposited in this way is much smaller than that of primary photon and thus the deposited energy is fluctuating significantly, that results in low DQE value. The efficiency for photons with spectrum 3 in 1cm thick Si detector is equal to $\sim 81\%$ while DQE is $\sim 42\%$.

Line spread function of the Si detector has been obtained by simulation with X-rays having energy distribution following spectrum 3 (Fig. 15). Spatial resolution of this detector is much better than of gaseous DIMEX. FWHM of the line spread function is $\sim 20\mu\text{m}$.

4. Conclusions.

5 years of operation of DIMEX at the SR beam-line at VEPP-3 has proven that the method of imaging of radiation from separate electron bunches is a very powerful tool. However in spite of successful application of the detector to the direct absorption imaging of detonation process and SAXS experiments, further improvement of the method is desirable. The development of new 5-pole 1.3T wiggler at VEPP-4M and construction of the new dedicated SR beam-line will allow the increase of energy and thus the thickness of samples under study. The simulation study performed in the present work demonstrates that the present detector will not change its parameters with the higher energy SR beam at VEPP-4M. The spatial resolution will stay at $\sim 0.2\text{mm}$ (FWHM) and DQE will be around 50%.

Spatial resolution of DIMEX and maximal X-ray flux that this detector can withstand are limited by the gaseous technology used in the present device. Further improvement of both parameters

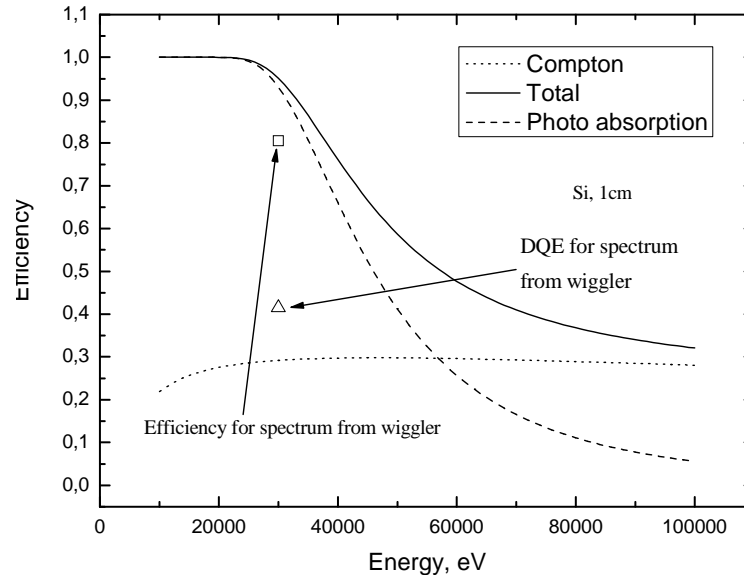


Figure 14. Efficiency of 1cm thick Si detector as a function of X-ray energy. Probability of a single interaction of one type (Compton or photo-) and of any type. Efficiency for the X-ray beam from 5-pole wiggler (spectrum 3) and DQE for the same radiation.

can be achieved by the development of solid-state DIMEX. Silicon microstrip detector could be a good candidate if it is positioned at a small angle to the beam. The simulation shows that if the beam crosses Si detector within 1cm length, the DQE for X-ray spectrum from VEPP-4M wiggler is close to that of the gaseous DIMEX. The spatial resolution is however can be much better if proper segmentation will be done, because the line spread function of the Si detector before the application of any strip readout structure is about $20\mu\text{m}$ wide (FWHM).

References

- [1] V.Aulchenko, P.Papushev, S.Ponomarev, L.Shekhtman and V.Zhulanov, *J.Synchrotron Rad.* (2003) 10, 361-365.
- [2] V. Aulchenko, O. Evdokov, S. Ponomarev, L. Shekhtman, K. Ten, B. Tolochko, I. Zhogin and V. Zhulanov, *Nucl.Instr.and Meth.* v.513, n.1-2 (2003) 388-393
- [3] V. Aulchenko, V. Zhulanov, L. Shekhtman, B. Tolochko, I. Zhogin, O. Evdokov and K. Ten, *Nucl.Instr.and Meth. A Volume 543*, n.1 (2005), 350-356.
- [4] E. R. Pruel, L. A. Merzhievskii, K. A. Ten, P. I. Zubkov, L. A. Luk'yanchikov, B. P. Tolochko, A. N. Kozyrev, and V. V. Litvenko, *Combustion, Explosion, and Shock Waves*, 2007. Vol. 43, No. 3, pp. 355-364.
- [5] V.M. Titov, B.P. Tolochko, K.A. Ten, L.A. Lukyanchikov, E. R. Pruel, *Diamond and Related Materials*. V.16, Issue 12, 2007, pp. 2009-2013

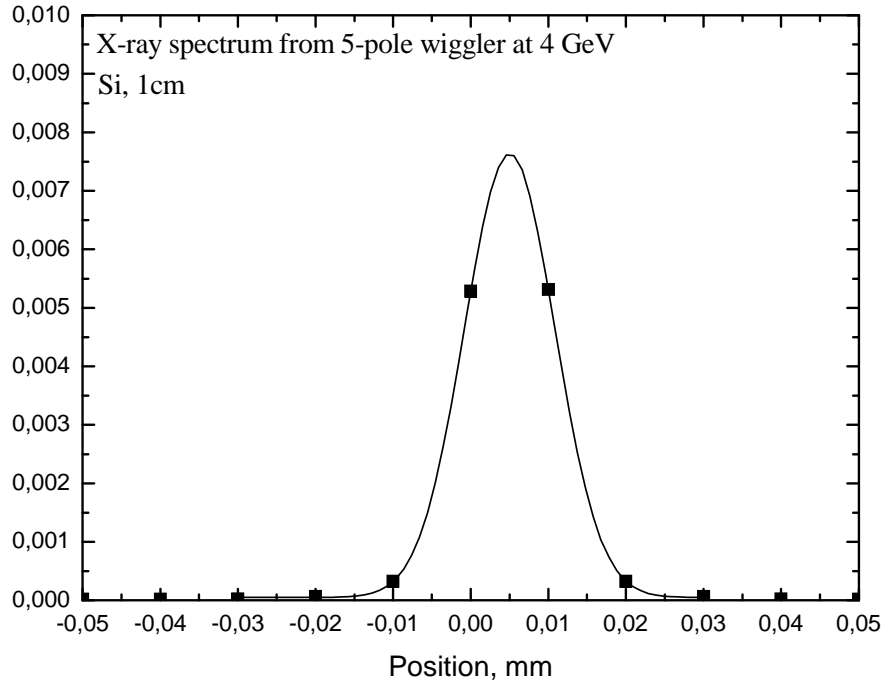


Figure 15. Line spread function of 1cm thick Si detector for photons with spectrum 3.

- [6] Horisberger, R. and Pitzl, D. (1993). Nucl. Instrum. Methods, A326, 92-99.
- [7] S. Bachmann, A. Bressan, L. Ropelewski, F. Sauli, A. Sharma, D. Mormann, Nucl. Instr. and Meth. A438(1999)376.
- [8] F. Sauli, L. Ropelewski and P. Everaerts, Nucl. Instr. and Meth. A560(2006)269
- [9] "FLUKA: a multi-particle transport code", A. Fasso, A. Ferrari, J. Ranft, and P.R. Sala, CERN-2005-10 (2005), INFN/TC-05/11, SLAC-R-773
- [10] "The physics models of FLUKA: status and recent developments", A. Fasso, A. Ferrari, S. Roesler, P.R. Sala, G. Battistoni, F. Cerutti, E. Gadioli, M.V. Garzelli, F. Ballarini, A. Ottolenghi, A. Empl and J. Ranft, Computing in High Energy and Nuclear Physics 2003 Conference (CHEP2003), La Jolla, CA, USA, March 24-28, 2003, (paper MOMT005), eConf C0303241 (2003), arXiv:hep-ph/0306267
- [11] J.C. Dainty and R. Shaw, Image Science: principles, analysis, and evaluation of photographic-type imaging processes, Academic Press, 1974.
- [12] Handbook of Medical Imaging. Volume 1. Physics and Psychophysics. Ed. Jacob Beutel, Harold L.Kundel, Richard L. Van Metter. SPIE Press, 2000.